JOURNAL OF THERMOPHYSICS AND HEAT TRANSFER
Vol. 12, No. 1, January–March 1998

Heat/Mass Transfer in a Rotating Two-Pass Channel with Transverse Ribs

C. W. Park* and S. C. Lau†
Texas A&M University, College Station, Texas 77843
and
R. T. Kukreja‡
Lynntech, Inc., College Station, Texas 77840

Naphthalene sublimation experiments have been conducted to study the local heat/mass transfer distributions on the rib-roughened leading and trailing walls of a rotating, two-pass, square channel, that models internal turbine blade cooling passages. The height of the transverse ribs was equal to one-tenth the spacing between the ribs, which was the same as the hydraulic diameter of the test channel. The Reynolds number and rotation number ranged up to 1 3 10^4 and 0.24, respectively. The results showed that, for radial outward flow in the first pass, there was very little spanwise variation of the local heat/mass transfer between consecutive ribs on the trailing wall. When the rotation number was high, however, there was significant spanwise variation on the leading wall, with high heat/mass transfer in the middle of the wall and very low heat/mass transfer near the two side walls. For radial inward flow in the second pass, the sharp turn reduced the difference between the heat/mass transfer on the leading wall and that on the trailing wall. The sharp turn also caused spanwise asymmetric variation of the local heat/mass transfer between consecutive ribs in the second pass immediately downstream of the turn. Relative to the heat/mass transfer in a corresponding stationary channel, the overall heat/mass transfer in a rotating channel with rib-roughened walls was not affected by the Coriolis force as much as that in a rotating channel with smooth walls.

Nomenclature

D = hydraulic diameter
h_m = local mass transfer coefficient, $\dot{M}''/(\rho_w - \rho_b)$
$\dot{M}''$ = local mass flux on naphthalene surface, $\rho_s \Delta z/\Delta t$
$\dot{m}$ = air mass flow rate
Nu = Nusselt number
Nu_0 = reference Nusselt number, $0.023Re^{0.8}Pr^{0.4}$
Pr = Prandtl number
R = mean rotating radius
Re = Reynolds number, $\dot{m}/(\mu D)$
Ro = rotation number, $\Omega D/U$
Sc = Schmidt number
Sh = local Sherwood number, $h_m D/\Lambda$
$\overline{Sh}$ = spanwise average Sherwood number
$\overline{Sh}$ = regional average Sherwood number
Sh_0 = reference Sherwood number, $0.023Re^{0.8}Sc^{0.4}$
U = average velocity of airflow
X = streamwise distance from mass transfer active channel inlet
Δt = duration of experiment
Δz = change of elevation at measurement point on naphthalene surface
$\Delta\rho/\rho$ = density ratio, $|(\rho_{\text{wall}} - \rho_{\text{inlet air}})|/\rho_{\text{inlet air}}$
Λ = diffusion coefficient of naphthalene vapor in air
μ = dynamic viscosity
ρ_b = bulk density of naphthalene vapor in airstream
ρ_s = density of solid naphthalene
ρ_w = vapor density of naphthalene at wall
Ω = rotational speed

Received March 17, 1997; revision received July 7, 1997; accepted for publication July 8, 1997.

*Postdoctoral Associate, Mechanical Engineering.
†Associate Professor, Mechanical Engineering.
‡Research Engineer, 7610 Eastmark Drive.

Introduction

IT is common for gas turbine blades to be cooled with air that flows through internal, shaped, rib-roughened, serpentine channels. The flow patterns in these channels and the heat transfer distributions on the channel walls are very different from those in stationary straight channels with smooth walls. Coriolis force pushes the airflow toward the various walls, depending on the flow direction and the channel orientation with respect to the rotating axis. The variation of density in the flow causes cross-streamwise variation of the buoyancy force, which generates secondary flow in the radial direction. At a sharp turn, the cooling air separates at the tip of the inner wall and centrifugal force causes flow impingement on the various walls at the turn. On the ribbed walls, the air separates at the top edges of the ribs and reattaches on the surfaces of the walls between ribs. The interactions among the forces in the flow caused by rotation, sharp turns, and ribs result in a highly complex flow pattern and large variations of the local heat transfer on the walls of a rotating, multipass, rib-roughened channel.

The dimensionless parameters governing the flowfield in a rotating frame are the Reynolds number, rotation number, and buoyancy parameter. These parameters may be considered as ratios of the inertial, viscous, Coriolis, and buoyancy forces. The rotation number plays a key role in determining the strength of the cross-streamwise secondary flow caused by the Coriolis force. The buoyancy parameter, which is equivalent to the ratio of the rotational Grashof number and the square of the Reynolds number, governs the radial secondary flow caused by buoyancy. Other factors that affect the heat transfer distribution, for airflow through a rotating multipass channel, include the flow entrance conditions, thermal boundary conditions, main flow direction, channel shape and orientation, geometries of the turns, and rib configuration.

Extensive heat transfer results are available in the literature for straight and multipass, smooth channels, rotating about perpendicular axes. These results were reviewed in detail in sev-

eral recent papers.[1,2] Among the benchmark results are those of Hajek et al.[3] and Wagner et al.,[4] who investigated the effects of Coriolis and buoyancy forces on the heat transfer in a multipass, square channel with smooth walls that were maintained at a uniform temperature.

Published results on heat transfer in straight and multipass, rib-roughened channels, rotating about perpendicular axes, were reviewed in recent publications.[5,6] El-Husayni et al.[7] conducted experiments to study the effect of boundary heat flux on the heat transfer in straight, square channels with smooth and turbulated walls. Wagner et al.[8] and Johnson et al.[9,10] investigated the heat transfer in multipass square channels with ribs normal and skewed to the flow. Johnson et al.[9] also studied the effect of model orientation on the heat transfer in rotating multipass square channels with ribbed walls. Parsons et al.[11] and Zhang et al.[12] presented results on the uneven wall temperature effect on the heat transfer in a two-pass square channel with normal and angled ribs.

Most of the published experimental results on heat transfer in rotating channels are regional average results. In this study, the detailed local heat transfer distributions on the walls of a rotating, two-pass, square channel are determined using the naphthalene sublimation technique and the heat/mass transfer analogy.[13] Attention is focused on the heat/mass transfer distributions on the two, rib-roughened, principal walls, i.e., the leading and trailing walls, of the test channel. The main objective of this study is to make available detailed local experimental heat/mass transfer data to enable better understanding of the effects of rotation, a sharp turn, and ribs on the local heat/mass transfer distribution in a rotating, two-pass channel, and to help improve the design of serpentine cooling channels in the gas turbine blades.

In the present mass transfer experiments, both the test section walls and the naphthalene vapor–air mixture that flows through the test section are at room temperature. Furthermore, the maximum naphthalene vapor concentration at the solid naphthalene surface is very small, such that the maximum variation of the density of naphthalene vapor–air mixture is only about 0.05%. Therefore, the density variation effect is negligible, and the present investigation examines only the effects of the Coriolis force, the turn, and the ribs, but not the buoyancy force, on the local heat/mass transfer distributions on the leading and trailing walls of a channel that models internal turbine blade cooling passages.

Test Apparatus and Procedure

The test section was an all-aluminum, two-pass channel with a sharp 180-deg turn. It had a square flow cross section (1.59 by 1.59 cm) and two, seven-hydraulic-diameter (11.11 cm) long, straight segments. The test section had seven separate walls: two principal walls, two inner walls (with their backs pressed against each other), two outer side walls, and an end wall (Fig. 1a). Naphthalene in a shallow cavity covered the inner surface of each wall. Each wall was designed and constructed so that none of the rims of the wall was exposed to the flowing air during an experiment. Once these walls were assembled, the interior surfaces of the test section were all mass transfer active, and the total thickness of the two inner walls was one-half of the channel hydraulic diameter (0.79 cm).

Ribs were cut from square balsa wood strips. They were attached transversely with epoxy on the straight segments of the two principal walls. The rib spacing, or the pitch, was equal to the hydraulic diameter of the test channel, which was also the channel width.

The seven walls of the test section were assembled inside a rectangular aluminum housing that had two parallel square channels separated by a 0.79-cm-thick wall (Fig. 1a). Once the seven individual walls were secured inside this housing, the assembly consisted of an entrance channel, the two-pass test channel, and an exit channel. The entrance and exit channels

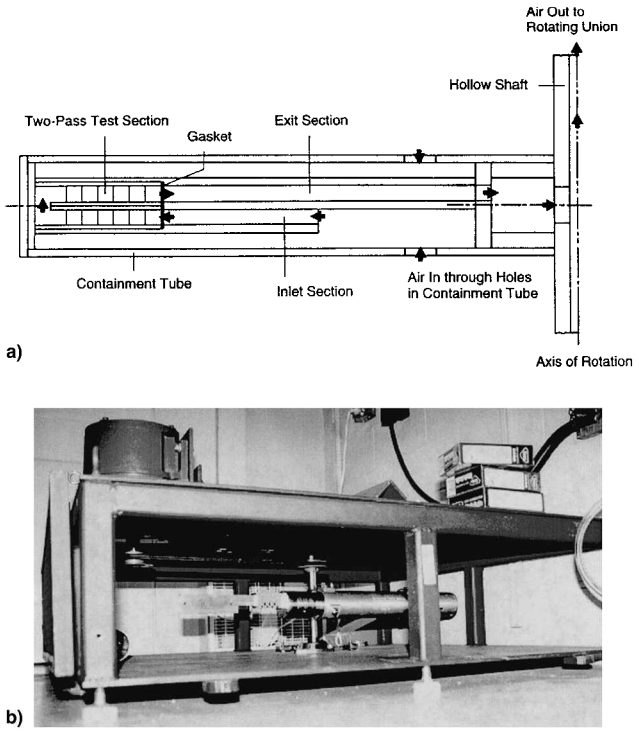

Fig. 1 a) Schematic of the two-pass test channel in the entrance/test/exit channel assembly and b) rotation test rig.

had the same square cross section as the test section, and had lengths of 10 and 20 hydraulic diameters, respectively. The end of this assembly with the outlet of the exit channel was welded to a short horizontal aluminum tube that was affixed to the vertical steel shaft of a rotating test rig, such that the mean rotating radius of the test section was 30 times the channel hydraulic diameter. The seven separate walls of the test section and the containment tube were designed such that they might be assembled or disassembled very quickly to minimize extraneous mass losses from the naphthalene-coated walls.

Figure 1b shows the rotation test rig with the rotating shaft supported by two bearings in a heavy steel cage. Not shown in Fig. 1 is an aluminum containment tube that enclosed the entire entrance/test/exit channel assembly (Fig. 1a). The entrance/test/exit channel assembly and the containment tube were balanced by an aluminum tube that was also welded to the short horizontal aluminum tube. The aluminum tube had the same diameter as the containment tube and was equipped with an adjustable sliding counterweight. A 5-hp electric motor drove the vertical shaft with a belt and two pulleys.

Also not shown in Fig. 1b are removable heavy steel meshes that fenced the vertical faces of the steel cage. The meshes were reinforced on the inside with steel angles and thick plywood boards.

Air at room temperature was drawn through bleed holes on the containment tube and then through the entrance/test/exit section assembly with a centrifugal blower. The air then flowed through the hollow rotating shaft, a rotating union, a calibrated orifice flow meter for flow rate measurement, and a gate valve for flow rate control, before it was ducted to an exhaust hood.

To obtain the distributions of the local mass transfer coefficient on the two principal walls of the test section, the elevations at a grid of up to about 750 points on the surface of each wall were measured and recorded at the beginning and the end of each test run. To measure the surface contour on a test wall, the wall was affixed firmly on an $X-Y$ coordinate table that was equipped with stepper motors to traverse the test wall in a horizontal plane. An electronic depth gauge with a resolution of 2.5×10^{-4} mm was used to measure the surface elevations at the grid points. The depth gauge consisted of a

lever-type sensor connected to an electronic amplifier. The stepwise movement of the coordinate table and the recording of output data were controlled with a microcomputer that was equipped with an A/D board.

An electronic balance with a resolution of either 0.01 or 0.1 mg was used to weigh the seven walls. Two manometers measured the pressures at the orifice flow meter, and thermocouples measured the inlet air temperatures and the air temperature at the orifice flow meter. An electronic tachometer was used to measure the rotational speed.

A test run was initiated by weighing all the walls and by acquiring the initial elevations at the grid of points on the naphthalene-coated surface of each of the two principal walls. The test section and the containment tube were then quickly assembled. After the motor was switched on to rotate the test section at the desired angular velocity, air was drawn through the test section with the blower. A test run lasted 1–2 h. During the run, the airflow rate and the air temperatures were monitored and recorded periodically. At the end of the run, each wall was weighed and the elevations at the same grid of points were measured again.

Separate experiments were carried out to determine the correction to the local mass transfer that was necessary to account for convection mass losses during motor and blower startup and shutdown, and while the local and overall measurements were conducted.

Data Reduction

The local mass transfer coefficient is evaluated as

$$h_m = \dot{M}''/(\rho_w - \rho_b) \tag{1}$$

$\dot{M}''$ at each measurement point is evaluated from the density of solid naphthalene, the change of elevation during a test run, and the duration of the test run, after applying the correction that is necessary to account for the mass losses at the beginning and the end of the test run.

In Eq. (1), ρ_w, is calculated using the ideal gas law along with the vapor pressure-temperature relation for naphthalene according to Eq. (1) in Ambrose et al.[14] Because the naphthalene vapor density at the wall is constant, the boundary condition on the naphthalene surfaces in this investigation corresponds to the thermal boundary condition of uniform wall temperature.

The bulk density at the inlet of the test section is zero. The values of the bulk density at the turn inlet and exit, and at the test section exit, are obtained from local surface contour measurements and the weights of the test section walls at the beginning and at the end of a test run, and the volumetric flow rate. ρ_b, at any streamwise location, is then determined as a piecewise linear function of the streamwise coordinate using the bulk density values at the inlet and exit of the test section, and at the turn.

The Sherwood number is

$$Sh = h_m D/\Lambda \tag{2}$$

Λ is calculated by Eq. (1) in Goldstein and Cho.[13] The corresponding Schmidt number is about 2.28.

If the local bulk density values are calculated as a linear function of the streamwise coordinate using the ρ_b values at the inlet and exit of the test section only, the maximum deviations of the local Sherwood number values at the turn inlet and exit for all of the test runs are found to be 1.5 and 1.8%, respectively. These small differences show that the piecewise linear bulk density distribution and the linear bulk density distribution (using the values at four locations) give local Sherwood number values that differ only very slightly, well within the estimated uncertainty of the local Sherwood number.

The Sherwood number is normalized by the corresponding Sherwood number for fully developed turbulent flow through a stationary smooth tube, $Sh_o = 0.023Re^{0.8}Sc^{0.4}$. Because rotation, sharp turns, and ribs affect the temperature and concentration fields, in a rotating multipass channel, in the same manner, through the velocity field, the following generalized heat/mass transfer analogy may be employed:

$$Nu/Nu_o = Sh/Sh_o \tag{3}$$

where $Nu_o = 0.023Re^{0.8}Pr^{0.4}$. Therefore, the normalized Sherwood number in this study may be considered as the comparison between the heat transfer coefficient for turbulent flow in a rotating two-pass square channel and that for corresponding fully developed turbulent flow in a stationary tube with a hydraulic diameter equal to that of the square channel.

The uncertainty of the Reynolds number is found to be 4.8%. The uncertainty of the local mass transfer coefficient depends on the uncertainties of the local wall and bulk naphthalene vapor densities and their difference, and the net local mass flux. A 0.56°C deviation in the surface temperature changes the naphthalene vapor density at the surface by as much as 6%. The measured temperatures varied within this range during a test run of 1–2 h. Δz ranged from 0.05 to 0.2 mm in most of the test runs. The bulk naphthalene vapor density at the test channel exit is found to be between 20 and 35% of the wall naphthalene vapor density. In calculating the uncertainty of the bulk density at a streamwise location, a maximum deviation of 5% of the wall density is estimated from the linearly interpolated value. Based on the method in Kline and McClintock,[15] the maximum uncertainty of the Sherwood number is estimated to be 12.2%.

Results

The detailed local heat/mass transfer distributions have been determined on the leading and trailing walls of the two-pass square test channel, for three Reynolds numbers of 5.5×10^3, 1×10^4, and 1.45×10^4, four rotation numbers of 0.0, 0.09, 0.16, and 0.24, and various rib sizes and configurations, with ribs on the various surfaces of the leading and trailing walls in the two straight passes of the test channel. The Reynolds number and rotation number ranges correspond to mean flow velocities up to 14.0 m/s and rotational speeds up to 770 rpm. In all, 50 different test conditions have been examined. The detailed local results of most of the test runs have been reported in Park.[6] The results presented here are only those for selected test runs in the case of transverse ribs with height that is equal to one-tenth of the pitch, or one-tenth of the channel hydraulic diameter.

In this section, the local heat/mass transfer distributions are presented as filled contours of the Sherwood number ratio on the leading and trailing walls of the two-pass square test channel. The local Sherwood number ratio is determined at up to about 1500 points on the two principal walls, using a grid of 54 points between consecutive ribs and 96 points at the turn. However, because of the finite size of the tip of the measuring probe of the depth gauge, local data are not available at locations very close to the edges of the walls and the bases of the ribs.

The spanwise average Sherwood number ratios $\overline{Sh}/Sh_o$, on the leading and trailing walls, are presented along a streamwise coordinate X/D. For the two straight passes of the test channel, $0 \le X/D \le 7$ and $9.5 \le X/D \le 16.5$, the values of the local Sherwood number ratio at nine spanwise distributed points at a given X/D are averaged to give the spanwise average value. In the turn, the values of the local Sherwood number ratio are averaged over three regions: 1) at 36 distributed measurement points in an upstream square region with an area of D^2, 2) 24 points in a middle rectangular region with an area of $0.5D^2$, and 3) 36 points in a downstream square region with an area of D^2. These regions are considered to be located at $X/D = 7.5$, 8.25, and 9.0.

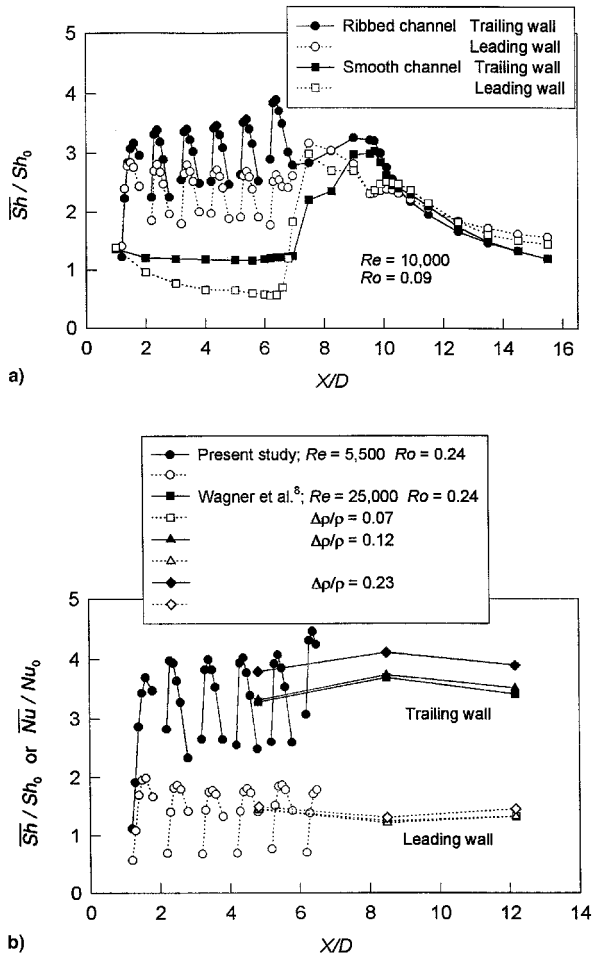

Fig. 2 a) Streamwise variations of $\overline{Sh}/Sh_0$ in two-pass square channels with smooth walls and with rib-roughened walls in the first pass: Re = 1 3 10^4 and Ro = 0.09 and b) comparison of the streamwise variations of $\overline{Sh}/Sh_0$ in this study with those of $\overline{Nu}/Nu_0$ from Wagner et al.[8]

In the following graphical presentation of the streamwise distributions of the regional mass transfer, open and darkened symbols are used to indicate the Sherwood number ratios on the leading and the trailing walls, respectively.

Smooth and Rib-Roughened Channels

In Fig. 2a, the streamwise variations of the regional Sherwood number ratios on the leading and trailing walls of a rotating rib-roughened channel are compared with those on the walls of a rotating smooth channel, for $Re = 1 \times 10^4$ and $Ro = 0.09$. In the rib-roughened channel, there are transverse ribs between $X/D = 1.0$ and = 6.0 on the leading and trailing walls in the first pass only. Figure 2a clearly shows that the mass transfer is very high where the flow reattaches on the walls between two transverse ribs, and that the ribs enhance the overall mass transfer on the leading and trailing walls. With rotation, the values of $\overline{Sh}/Sh_0$ on the trailing walls in the first passes of both the smooth and the rib-roughened channels are higher than corresponding values on the leading walls. In each channel, the rotation-induced Coriolis force in the radial outward flow pushes the high momentum core fluid toward the trailing wall with accompanying pressure gradient across the channel cross section. The pressure field drives the low-momentum fluid near the inner and outer walls toward the leading wall, forming double vortices. The higher mass transfer on the trailing wall and the lower mass transfer on the leading wall are primarily caused by the shift of the high-velocity, low-concentration core flow toward the trailing wall. The shift causes larger velocity and concentration gradients near the trailing wall and smaller gradients near the leading wall.

In the upstream region of the smooth turn (at $X/D = 7.5$) in each of the two channels, the leading wall mass transfer increases abruptly and is higher than the trailing wall mass transfer. The high mass transfer on the leading wall is believed to be the result of the interaction between the rotation-induced vortices and the turn-induced vortex pair, which strengthens the turn-induced vortex nearer the leading wall, and forces much of the low concentration core flow to wash the end wall and then the outside portion of the leading wall.

In the downstream region of the turn (at $X/D = 9.0$), the mass transfer is high on both the leading and trailing walls. In the smooth second pass in each channel, the mass transfer on both walls decreases with distance from the turn, as the flow redevelops. With radial inward flow in the second pass, rotation increases the leading wall mass transfer and decreases the trailing wall mass transfer. Figure 2a shows that, for $Re = 1 \times 10^4$ and $Ro = 0.09$, the ribs in the first pass increase the mass transfer on the smooth leading and trailing walls in the turn. However, the ribs do not affect the shapes of the mass transfer distributions on the smooth leading and trailing walls in the second pass, suggesting that there is a strong dependency of the flowfield on the geometry of the sharp turn.

The overall averages of the Sherwood number values in the first pass of a rotating rib-roughened channel under various test conditions are normalized with the corresponding overall averages in the first pass of a stationary rib-roughened channel. Similarly, the overall averages of the Sherwood number values in the first pass of a rotating smooth channel under various test conditions are normalized with the corresponding overall averages in the first pass of a stationary smooth channel. When these overall normalized Sherwood number values are compared, it becomes clear that, for the radial outward flow, rotation increases the mass transfer (relative to stationary channel mass transfer) on the trailing wall and decreases that on the leading wall of a smooth channel more than that on corresponding walls of a rib-roughened channel.

For instance, using the results in the case of $Re = 1 \times 10^4$ and $Ro = 0.09$ that are presented in Fig. 2a, the values of $\overline{Sh}/Sh_0$ are averaged over the rib pitch between $X/D = 5.0$ and 6.0. These regional average values are then compared with corresponding values based on the results for stationary smooth and rib-roughened channels. It is found that, in the smooth channel case, rotation decreases the leading-wall mass transfer by 45% and increases the trailing-wall mass transfer by 31%. On the other hand, in the ribbed channel case, rotation decreases the leading-wall mass transfer by only 21% and increases the trailing-wall mass transfer by only 14%. The near-wall secondary flow that is caused by the ribs may lessen the propagation of the core flow toward the trailing wall, reducing the asymmetry of the radial velocity profile.

Comparison with Published Results

In Fig. 2b, the $\overline{Sh}/Sh_0$ distributions on the leading and trailing walls of the first pass in the case of $Re = 5.5 \times 10^3$ and $Ro = 0.24$ are compared with the corresponding $\overline{Nu}/Nu_0$ distributions by Wagner et al.[8] The rotating channel in Wagner et al.[8] had a very short unheated entrance channel, 14 hydraulic-diameter long straight passes, and a mean rotation radius of 49 times the hydraulic diameter. The $\overline{Nu}/Nu_0$ distributions in Fig. 2b are for $Re = 2.5 \times 10^4$, $Ro = 0.24$, and density ratios of 0.07, 0.12, and 0.23. Despite differences in the test conditions of the two studies and negligible buoyancy variation effect in this study, the $\overline{Sh}/Sh_0$ distributions compare very well with the published $\overline{Nu}/Nu_0$ distributions. Johnson et al.[9] reported that buoyancy affected the heat transfer in a rotating rib-roughened channel less than that in a rotating smooth channel.

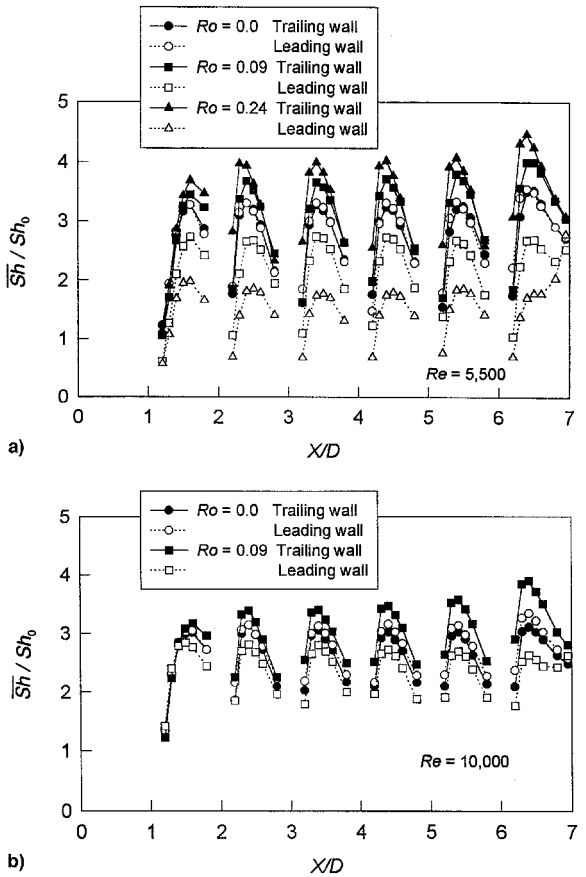

Fig. 3 Effect of rotation on the streamwise variations of $\overline{Sh}/Sh_0$ in a two-pass square channel with rib-roughened walls: a) Re = 5.5 3 10^3 and Ro = 0.0, 0.09, and 0.24 and b) Re = 1 3 10^4 and Ro = 0.0 and 0.09.

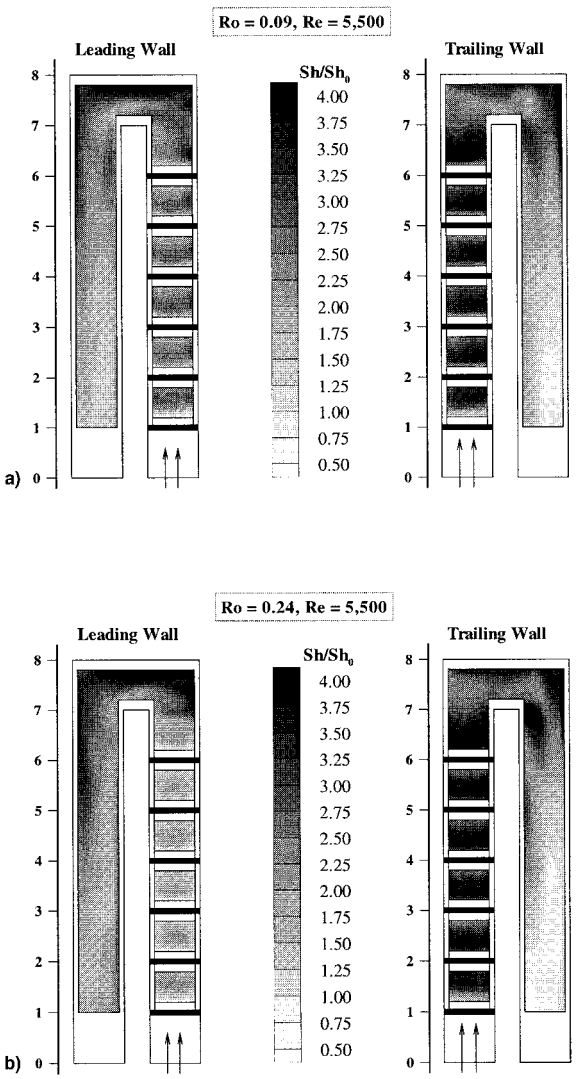

Fig. 4 Local Sh/Sh_0 distributions in a two-pass square channel: a) Re = 5.5 3 10^3 and Ro = 0.09 and b) Re = 5.5 3 10^3 and Ro = 0.24.

Effect of Rotation Number

To study the effect of rotation on the mass transfer on the leading and trailing walls of a rotating rib-roughened channel, the $\overline{Sh}/Sh_0$ distributions for $Re = 5.5 \times 10^3$ and Ro = 0.0, 0.09, and 0.24, and for $Re = 1 \times 10^4$ and Ro = 0.0 and 0.09, are presented in Figs. 3a and 3b, respectively. Attention is focused on the mass transfer in the first straight pass only. Figures 3a and 3b show that increasing the rotation number increases the $\overline{Sh}/Sh_0$ values on the trailing wall, and decreases the $\overline{Sh}/Sh_0$ values on the leading wall. The $\overline{Sh}/Sh_0$ distributions between consecutive ribs are all similar, except for that between the first two ribs near the channel entrance. Increasing the rotation number increases the Coriolis force that pushes the core flow toward the trailing wall in the radial outward flow. The resulting velocity and concentration gradients near the trailing and leading walls cause the high mass transfer on the trailing wall and the low mass transfer on the leading wall.

Figures 4a and 4b give the distributions of the local mass transfer for $Re = 5.5 \times 10^3$ and Ro = 0.09 and 0.24, respectively. In the case of Ro = 0.09, the value of Sh/Sh_0 reaches about 3.75 on the trailing wall where the flow reattaches between two ribs, and only about 2.75 on the leading wall. When Ro = 0.24, the maximum value of Sh/Sh_0 on the trailing wall between two ribs is more than 4.0. There is very little spanwise variation of the Sh/Sh_0 distribution on the trailing wall. The Sh/Sh_0 distribution on the leading wall, however, shows significant spanwise variation with a typical maximum Sh/Sh_0 value of about 2.25 in the middle of the channel, and low values of below 1.50 near the two side walls. When the rotation number is high, the strengthened Coriolis force significantly lowers the flow velocity near the leading wall. There appears to be only a weak reattachment of the low-momentum near-wall flow over a rib on the leading wall. The flow near the edges of the leading wall is slowed further by the two side walls, resulting in the lower mass transfer near the edges of the leading wall than in the middle of the wall.

Figures 4a and 4b show that the Sh/Sh_0 distributions in the turn and in the second pass with smooth walls are not significantly affected by the ribs on the leading and trailing walls of the first pass. The very high mass transfer near the end wall on the leading wall, the high mass transfer immediately downstream of the second inner corner of the turn on the trailing wall, the low mass transfer at the second inner corner of the turn on the leading wall, and the generally high mass transfer on the outer wall immediately downstream of the second outer corner of the turn on both the leading and trailing walls, are all typical of the mass transfer distribution on a corresponding rotating two-pass square channel with smooth walls.[3]

Effect of Reynolds Number

The effect of varying the Reynolds number on the mass transfer distribution in the rib-roughened channel is demonstrated in Fig. 5. The spanwise-averaged Sherwood number ratio distributions are presented for $Re = 5.5 \times 10^3$ and 1×10^4, in the cases of Ro = 0.0 and 0.09, respectively. Attention is again focused on the mass transfer in the first straight pass only. Figure 5 show that the $\overline{Sh}/Sh_0$ distributions are not significantly affected by the Reynolds number, except that in-

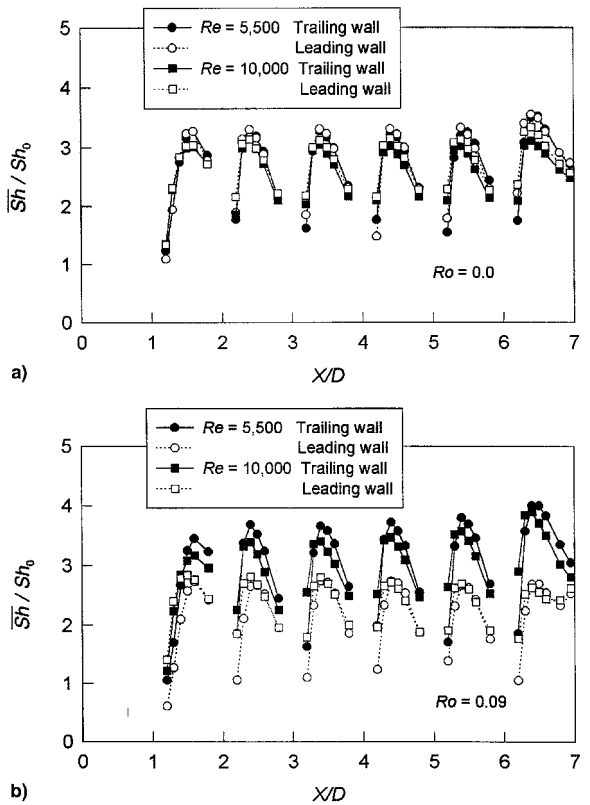

Fig. 5 Effect of Re on the streamwise variations of $\overline{Sh}/Sh_0$ in a two-pass square channel with rib-roughened walls: a) Re = 5.5 × 10^3 and 1 × 10^4, and Ro = 0.0 and b) Re = 5.5 × 10^3 and 1 × 10^4, and Ro = 0.09.

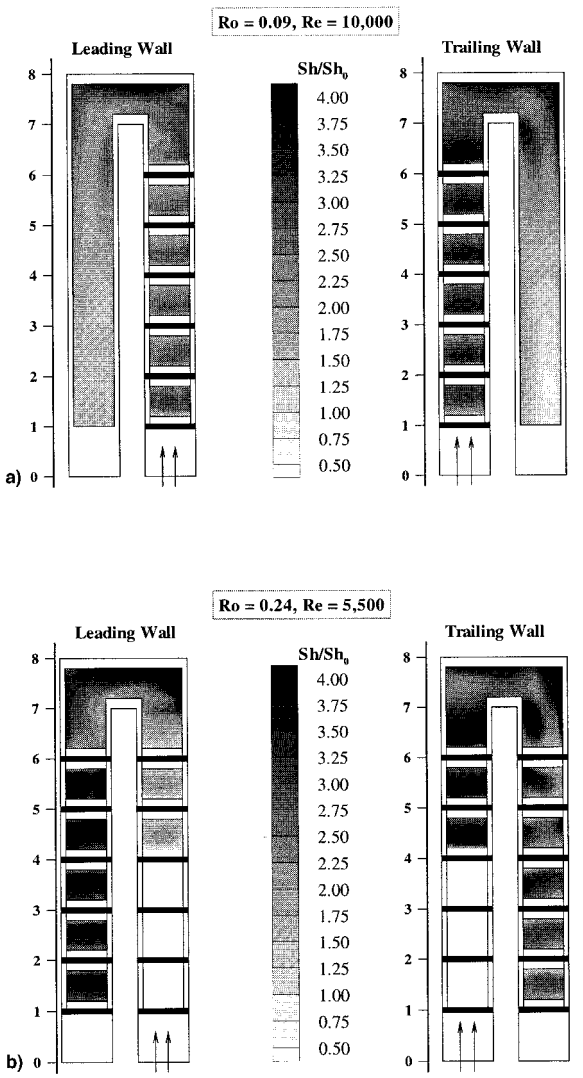

Fig. 6 Local Sh/Sh_0 distributions in a two-pass square channel: a) Re = 1 × 10^4 and Ro = 0.09 and b) Re = 5.5 × 10^3 and Ro = 0.24, with ribs on the leading and trailing walls of both the first and second passes.

creasing the Reynolds number lessens slightly the streamwise variation of $\overline{Sh}/Sh_0$ between two ribs.

Figure 6a displays the distributions of the local mass transfer for $Re = 1 \times 10^4$ and $Ro = 0.09$. Comparing Figs. 4a and 6a, it is evident that the patterns of the local mass transfer distributions do not change significantly when the Reynolds number is changed from 5.5×10^3 to 10^4.

Effect of Ribs in Second Pass

Figure 6b displays the distributions of the local mass transfer for $Re = 5.5 \times 10^3$ and $Ro = 0.24$, in a channel with ribs on the leading and trailing walls of both the first and second passes. Comparing Figs. 4b and 6b, it is evident that the Sh/Sh_0 distributions in the first pass and in the turn are not affected by the ribs in the second pass. In the second pass, with the reversal of the Coriolis force in the radial inward flow, the mass transfer is very high on the leading wall between two ribs and is relatively low on the trailing wall between two ribs. However, the trailing wall mass transfer in the second pass is significantly higher than the leading wall mass transfer in the first pass. Therefore, the sharp turn reduces the difference between the mass transfer on the leading wall and that on the trailing wall, which is the result of the rotation-induced secondary flow. Furthermore, the turn causes significant spanwise variation of the mass transfer on the trailing wall in the second pass immediately downstream of the turn; the variation lessens gradually, as the flow redevelops in the second pass.

Effect of Ribs on Regional Average Mass Transfer

The overall averages of the $\overline{Sh}/Sh_0$ values between the ribs at X/D = 4.0 and 6.0, on the leading and trailing walls in the first straight pass, and between the ribs at X/D = 13.5 and 15.5, on the leading and trailing walls in the second straight pass, for $Re = 5.5 \times 10^3$ and $Ro = 0.24$, are calculated. Similarly, the overall averages of the smooth wall $\overline{Sh}/Sh_0$ values between X/D = 4.0 and 6.0, and between X/D = 13.5 and 15.5, on the leading and trailing walls, for $Re = 5.5 \times 10^3$ and $Ro = 0.24$, are obtained. It is found that, in the ribbed channel case, $\overline{Sh}/Sh_0$ = 1.48 and 3.26 on the leading and trailing walls of the first pass, and $\overline{Sh}/Sh_0$ = 3.28 and 2.37 on the leading and trailing walls of the second pass, respectively. In the smooth channel case, $\overline{Sh}/Sh_0$ = 0.4 and 1.60 on the leading and trailing walls of the first pass, and $\overline{Sh}/Sh_0$ = 1.79 and 1.00 on the leading and trailing walls of the second pass, respectively.

These regional average results again show that transverse ribs enhance the mass transfer on the leading and trailing walls, and rotation-induced Coriolis force increases the mass transfer on the trailing wall for radial outward flow in the first pass and on the leading wall for radial inward flow in the second pass. Also, the sharp turn reduces the difference between the mass transfer on the leading and trailing walls in the second pass.

Concluding Remarks

The effects of Coriolis force, sharp turn, and transverse ribs on the local heat/mass transfer distributions on the leading and trailing walls of a rotating, two-pass, square turbine blade cooling channel model have been investigated. The height of the ribs was equal to one-tenth the spacing between the ribs, which was the same as the hydraulic diameter of the test channel.

Experiments were conducted with $Re = 5.5 \times 10^3$ and 1×10^4, and $Ro = 0.0$, 0.09, and 0.24. Based on the results obtained under these test conditions, the following conclusions are drawn:

1) For radial outward flow in the first pass, increasing the rotation number increases the heat/mass transfer between consecutive ribs on the trailing wall and decreases that on the leading walls. There is very little spanwise variation of the local heat/mass transfer between consecutive ribs on the trailing wall. When the rotation number is high, however, there is significant spanwise local heat/mass transfer variation on the leading wall, with high heat/mass transfer in the middle of the wall and very low heat/mass transfer near the two side walls.

2) For radial inward flow in the second pass, the heat/mass transfer between consecutive ribs is very high on the leading wall and is relatively low on the trailing wall. However, the trailing wall heat/mass transfer in the second pass is significantly higher than the leading wall heat/mass transfer in the first pass. The sharp turn reduces the difference between the heat/mass transfer on the leading wall and that on the trailing wall. The sharp turn also causes spanwise asymmetric variation of the local heat/mass transfer between consecutive ribs in the second pass immediately downstream of the turn.

3) Compared with the heat/mass transfer distributions in a channel with smooth walls, the ribs on the leading and trailing walls of the two straight passes increase the variations of the heat/mass transfer on the walls between two ribs, but do not significantly change the shapes of the local heat/mass transfer distributions on the smooth walls in the turn.

4) Relative to the heat/mass transfer in a corresponding stationary channel, the overall heat/mass transfer in a rotating channel with rib-roughened walls is not affected by the Coriolis force as much as that in a rotating channel with smooth walls.

5) Varying the Reynolds number does not significantly change the shapes of the local heat/mass transfer distributions on the rib-roughened leading and trailing walls.

Acknowledgments

This study was sponsored by NASA Lewis Research Center, Cleveland, Ohio, Grant NAS3-27739, and the Center for Energy and Mineral Resources, College Station, Texas.

References

[1]Kuo, C. R., and Hwang, G. J., "Experimental Studies and Correlations of Radially Outward and Inward Air-Flow Heat Transfer in a Rotating Square Duct," *Journal of Heat Transfer*, Vol. 118, Feb. 1996, pp. 23–30.

[2]Park, C. W., Kandis, M., and Lau, S. C., "Heat/Mass Transfer Distribution in a Rotating Two-Pass Square Channel—Part I: Regional Heat Transfer, Smooth Channel," *International Journal of Rotating Machinery*, 1997 (to be published).

[3]Hajek, T. J., Wagner, J. H., Johnson, B. V., Higgens, A. W., and Steuber, G. D., "Effects of Rotation on Coolant Passage Heat Transfer: Volume I—Coolant Passages with Smooth Walls," NASA CR 4396, Sept. 1991.

[4]Wagner, J. H., Johnson, B. V., and Kopper, F. C., "Heat Transfer in Rotating Serpentine Passages with Smooth Walls," *Journal of Turbomachinery*, Vol. 113, July 1991, pp. 321–330.

[5]Tse, D. G. N., and Steuber, G., "Flow in Rotating Serpentine Coolant Passages with Skewed Trip Strips," NASA CR 198530, Oct. 1996.

[6]Park, C. W., "Local Heat/Mass Transfer Distributions in Rotating Two-Pass Square Channels," Ph.D. Dissertation, Dept. of Mechanical Engineering, Texas A&M Univ., College Station, TX, Dec. 1996.

[7]El-Husayni, H. A., Taslim, M. E., and Kercher, D. M., "Experimental Heat Transfer Investigation of Stationary and Orthogonally Rotating Asymmetric and Symmetric Heated Smooth and Turbulated Channels," *Journal of Turbomachinery*, Vol. 116, Jan. 1994, pp. 124–132.

[8]Wagner, J. H., Johnson, B. V., Graziani, R. A., and Yeh, F. C., "Heat Transfer in Rotating Passages with Trips Normal to the Flow," *Journal of Turbomachinery*, Vol. 114, Oct. 1992, pp. 847–857.

[9]Johnson, B. V., Wagner, J. H., and Steuber, G. D., "Effects of Rotation on Coolant Passage Heat Transfer: Volume II—Coolant Passages with Trips Normal and Skew to the Flow," NASA CR 4396, Oct. 1993.

[10]Johnson, B. V., Wagner, J. H., Steuber, G. D., and Yeh, F. C., "Heat Transfer in Rotating Serpentine Passages with Trips Skewed to the Flow," *Journal of Turbomachinery*, Vol. 116, Jan. 1994, pp. 113–123.

[11]Parsons, J. A., Han, J. C., and Zhang, Y. M., "Wall Heating Effect on Local Heat Transfer in a Rotating Two-Pass Square Channel with 90° Rib Turbulators," *International Journal of Heat and Mass Transfer*, Vol. 37, Sept. 1994, pp. 1411–1420.

[12]Zhang, Y. M., Han, J. C., Parsons, J. A., and Lee, C. P., "Surface Heating Effect on Local Heat Transfer in a Rotating Two-Pass Square Channel with 60 Deg Angled Rib Turbulators," *Journal of Turbomachinery*, Vol. 117, April 1995, pp. 272–280.

[13]Goldstein, R. J., and Cho, H. H., "A Review of Mass Transfer Measurements Using Naphthalene Sublimation," *Experimental Thermal and Fluid Science*, Vol. 10, May 1995, pp. 416–434.

[14]Ambrose, D., Lawrenson, I. J., and Sprake, C. H. S., "The Vapor Pressure of Naphthalene," *Journal of Chemical Thermodynamics*, Vol. 7, Dec. 1975, pp. 1173–1176.

[15]Kline, S. J., and McClintock, F. A., "Describing Uncertainties in Single Sample Experiments," *Mechanical Engineering*, Vol. 75, Jan. 1953, pp. 3–8.